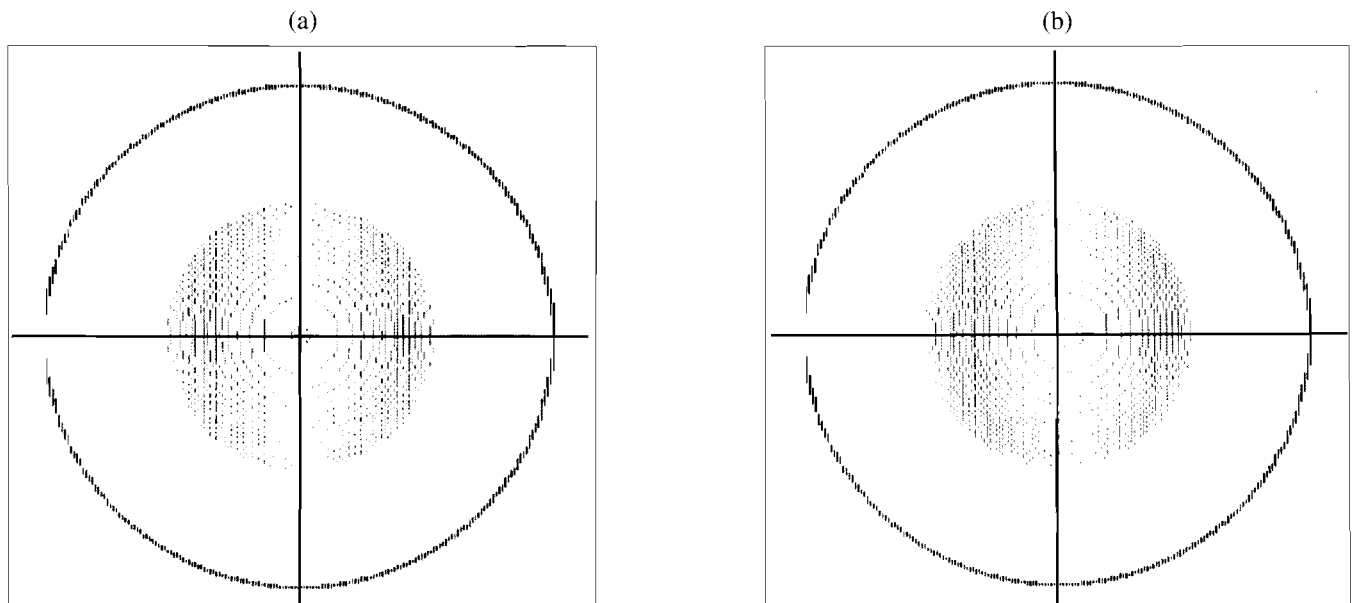


Characterization of Thick Cryogenic Fuel Layers: Compensation for the Lens Effect Using Convergent Beam Interferometry

Historically, the fuel content and fuel-layer uniformity of cryogenic targets have been characterized interferometrically using plane-wave illumination.¹⁻⁶ This technique has the sensitivity necessary to detect a deviation from sphericity of the fuel layer's inside surface as small as a few percent of its total thickness. In the past at LLE, the targets examined were typically 250- μm -diam glass capsules with wall thicknesses of a few micrometers that were filled with enough fuel to produce a condensed fuel layer less than 10 μm in thickness. Future OMEGA Upgrade cryogenic targets will consist of polymer capsules several tens of micrometers thick with diameters ranging from 700–1100 μm . These will be filled with condensed D₂ or DT fuel with a thickness of up to 100 μm .

A capsule with a thick cryogenic layer condensed on its interior behaves as a strong negative lens, which has several adverse effects on its interferogram when created with plane-wave illumination. Computer simulations of typical interferograms are shown in Fig. 58.24. The highly divergent and spherically aberrated wavefront created by the target cannot be effectively collected and imaged using optics with convenient numerical apertures, resulting in loss of information near the perimeter of the target's image. In addition, when this highly curved wavefront interferes with a planar reference wavefront, an interferogram with a fringe spatial frequency that increases radially to very high values near the perimeter of the target's image is produced. Since the phase, and therefore



T1083

Figure 58.24

Computer-generated interferograms of a 10- μm -thick polystyrene capsule with a diameter of 1120 μm that contains 100 μm of condensed fuel. These were created with the assumptions that both the object and reference beams consisted of planar wavefronts with a 514-nm wavelength, and $f/6$ optics were used to image the target. All of the surfaces in (a) are perfectly concentric with one another, whereas (b) displays a 5% fuel nonconcentricity, i.e., the center of the spherical inner surface of the condensed fuel layer has been displaced to the right in the figure by 5% of its total thickness. Obviously, a 5% nonconcentricity can be easily detected, but higher-order nonuniformities are much more difficult to detect due to the very high fringe frequency. In addition, information regarding the state of the fuel near the perimeter of the target's image has been lost due to refraction of the object beam outside of the imaging optics' finite collection aperture.

thickness, resolution resulting from the analysis of an interferogram is inversely proportional to the number of detector elements per fringe, the phase sensitivity is reduced dramatically when the fringe frequency approaches the Nyquist limit of the detector. As the fringe frequency nears the frequency of pixels in the CCD array, aliasing occurs and the fringes become unresolved. Evidence of this is the Moiré patterns exhibited in the theoretical interferograms of Fig. 58.24, where the fringes are beating with their array locations instead of CCD detector elements.

There are several requirements of a cryogenic-target interferometer that are applicable to OMEGA Upgrade target experiments. First, it should be sensitive to high-order fuel nonuniformities, not only nonconcentricity of the inner and outer fuel-layer surfaces. It should also be suitable for a wide range of capsule/fuel-layer dimensions. It should be simple to implement, optically stable, and amenable to computerized wavefront-measuring techniques (i.e., phase-shifting interferometry) to obtain the most accurate quantitative information possible. Finally, it should be compact and versatile enough to be adapted to *in-situ* fuel-layer characterization both in laboratory and target chamber experiments.

To realize these requirements, an interferometer has been developed that illuminates the target with a wavefront that is convergent to a point near the target's rear focal point, thus causing a nearly planar wavefront to emerge from it. A comparison between the emergent wavefront with plane-wave and convergent-beam illumination is shown in Fig. 58.25. With convergent-beam illumination, when the transmitted wavefront interferes with a planar reference wavefront, a low-fringe-

frequency interferogram of the target is produced that can be analyzed with a better phase resolution.

When imaged on axis, the wavefront emerging from the target with plane-wave illumination departs from a plane with two major components: a diverging spherical element designated as x_1 in Fig. 58.26 and a spherical aberration contribution designated as x_2 . In Fig. 58.26, f_{tgt} is the effective focal length of the target as measured from the capsule's equatorial plane (i.e., the y -axis), examples of which are given as a function of fuel-layer thickness for a 10- μm -thick polystyrene capsule in Fig. 58.27. For $(r/f_{\text{tgt}})^2 \ll 1$, where r is the inner radius of the condensed fuel layer, x_1 can be approximated as parabolic: $x_1 = (r^2/2f_{\text{tgt}})y^2$, while x_2 depends on y to the fourth power as $x_2 = W_{040}y^4$. The optical system collects and images this transmitted wavefront and the capsule. Since the perimeter of the target's image is normally in focus in an interferogram, the emergent wavefront is imaged as if projected back into the equatorial plane of the target; hence y is the normalized pupil function and is given by the ratio of the distance from the center of the target's image to the inner radius of the fuel layer r . Therefore, if x_1 is eliminated by illuminating the target with a wavefront converging to a point behind it, a distance f_{tgt} away from its center, only the spherically aberrant component of the transmitted wavefront remains. This flattens the wavefront emerging from the target, with only the curvature due to the spherical aberration term left. By using convergent-beam illumination, not only is more light collected from regions near the perimeter of the target, but the interferogram consists of fewer rings that are concentrated near the perimeter of the target's image, decreasing the maximum fringe frequency to a value well below the Nyquist limit of the detector array.

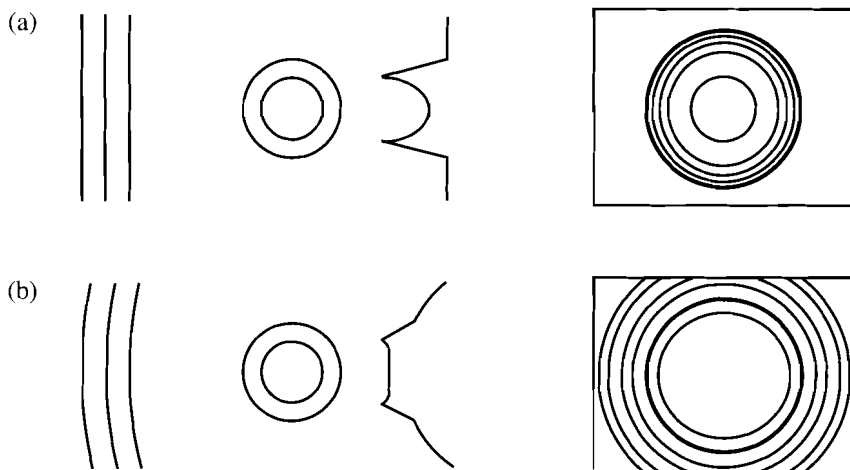


Figure 58.25

An illustration of the wavefront that emerges from a capsule filled with a thick condensed fuel layer when both plane-wave and convergent-beam illumination are used, along with hypothetical interferograms that are produced when the transmitted wavefront interferes with a planar reference wavefront. It is apparent in (a) that a relatively small portion of the highly divergent wavefront can be effectively collected and imaged. However, in (b), not only is the transmitted wavefront flattened, but the light surrounding the capsule can also be readily collected and imaged.

T1113

thickness, resolution resulting from the analysis of an interferogram is inversely proportional to the number of detector elements per fringe, the phase sensitivity is reduced dramatically when the fringe frequency approaches the Nyquist limit of the detector. As the fringe frequency nears the frequency of pixels in the CCD array, aliasing occurs and the fringes become unresolved. Evidence of this is the Moiré patterns exhibited in the theoretical interferograms of Fig. 58.24, where the fringes are beating with their array locations instead of CCD detector elements.

There are several requirements of a cryogenic-target interferometer that are applicable to OMEGA Upgrade target experiments. First, it should be sensitive to high-order fuel nonuniformities, not only nonconcentricity of the inner and outer fuel-layer surfaces. It should also be suitable for a wide range of capsule/fuel-layer dimensions. It should be simple to implement, optically stable, and amenable to computerized wavefront-measuring techniques (i.e., phase-shifting interferometry) to obtain the most accurate quantitative information possible. Finally, it should be compact and versatile enough to be adapted to *in-situ* fuel-layer characterization both in laboratory and target chamber experiments.

To realize these requirements, an interferometer has been developed that illuminates the target with a wavefront that is convergent to a point near the target's rear focal point, thus causing a nearly planar wavefront to emerge from it. A comparison between the emergent wavefront with plane-wave and convergent-beam illumination is shown in Fig. 58.25. With convergent-beam illumination, when the transmitted wavefront interferes with a planar reference wavefront, a low-fringe-

frequency interferogram of the target is produced that can be analyzed with a better phase resolution.

When imaged on axis, the wavefront emerging from the target with plane-wave illumination departs from a plane with two major components: a diverging spherical element designated as x_1 in Fig. 58.26 and a spherical aberration contribution designated as x_2 . In Fig. 58.26, f_{tgt} is the effective focal length of the target as measured from the capsule's equatorial plane (i.e., the y -axis), examples of which are given as a function of fuel-layer thickness for a 10- μ m-thick polystyrene capsule in Fig. 58.27. For $(rf_{tgt})^2 \ll 1$, where r is the inner radius of the condensed fuel layer, x_1 can be approximated as parabolic: $x_1 = (r^2/2f_{tgt})y^2$, while x_2 depends on y to the fourth power as $x_2 = W_{040}y^4$. The optical system collects and images this transmitted wavefront and the capsule. Since the perimeter of the target's image is normally in focus in an interferogram, the emergent wavefront is imaged as if projected back into the equatorial plane of the target; hence y is the normalized pupil function and is given by the ratio of the distance from the center of the target's image to the inner radius of the fuel layer r . Therefore, if x_1 is eliminated by illuminating the target with a wavefront converging to a point behind it, a distance f_{tgt} away from its center, only the spherically aberrant component of the transmitted wavefront remains. This flattens the wavefront emerging from the target, with only the curvature due to the spherical aberration term left. By using convergent-beam illumination, not only is more light collected from regions near the perimeter of the target, but the interferogram consists of fewer rings that are concentrated near the perimeter of the target's image, decreasing the maximum fringe frequency to a value well below the Nyquist limit of the detector array.

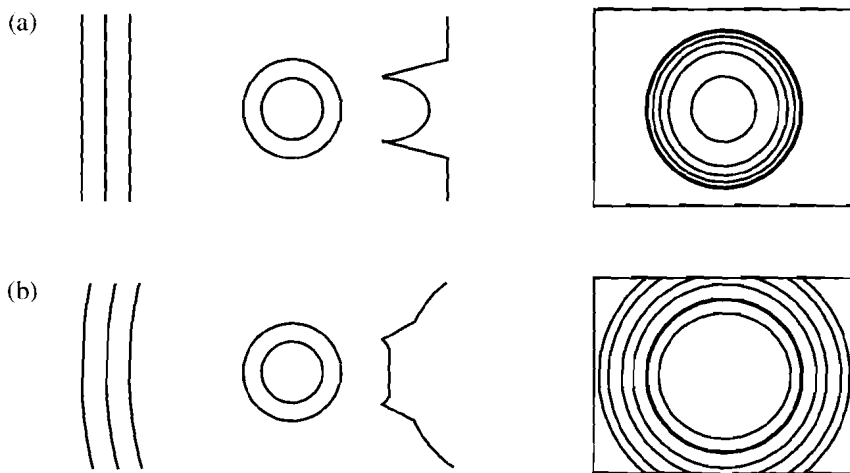
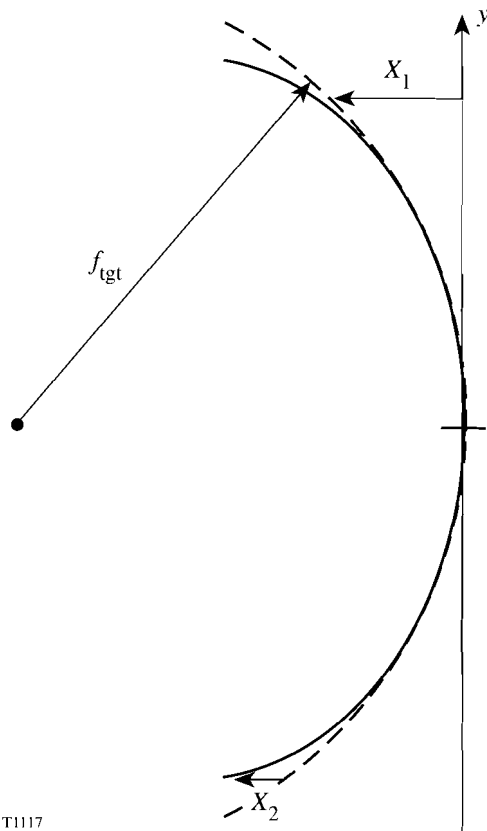


Figure 58.25
An illustration of the wavefront that emerges from a capsule filled with a thick condensed fuel layer when both plane-wave and convergent-beam illumination are used, along with hypothetical interferograms that are produced when the transmitted wavefront interferes with a planar reference wavefront. It is apparent in (a) that a relatively small portion of the highly divergent wavefront can be effectively collected and imaged. However, in (b), not only is the transmitted wavefront flattened, but the light surrounding the capsule can also be readily collected and imaged.

T1113

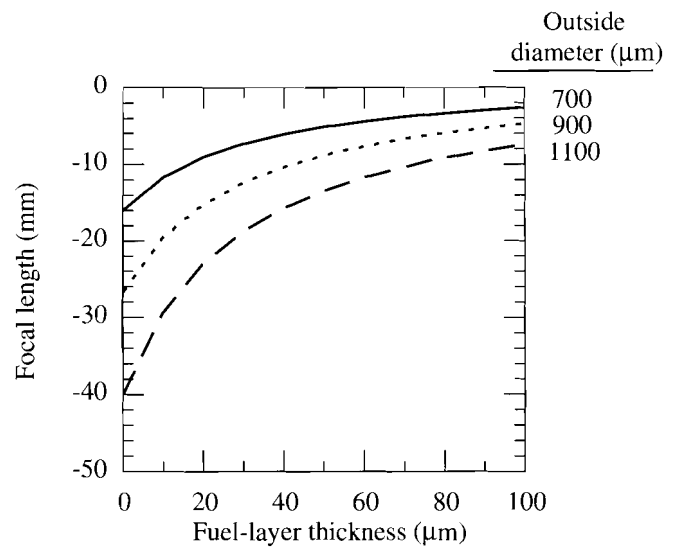


T1117

Figure 58.26

An illustration of the wavefront emerging from a cryogenic target when it is illuminated with a planar wavefront. The emergent wavefront is normally imaged as if projected back into the equatorial plane of the target, making the y -axis lie along a major diameter of the spherical inner surface of the condensed fuel layer. The transmitted wavefront contains two major components: a diverging spherical constituent designated as x_1 and a spherical aberration term designated as x_2 , and f_{tgt} is the effective focal length of the target.

The values for $r^2/2f_{tgt}$ and W_{040} in Fig. 58.28 were calculated by tracing paraxial rays through a hypothetical cryogenic target to find its focal length and applying third-order aberration theory to determine the spherical aberration component. The values shown are for the emerging wavefront projected back into the equatorial plane of the target and denote the maximum values these quantities take, i.e., for $y = 1$. The number of fringes present in an interferogram between the center of a target's image and a point along its radius can readily be determined from Fig. 58.28 by summing x_1 and x_2 for a given y and dividing by the wavelength of the light used to create it. For example, a 10- μm -thick polystyrene capsule with a diameter of 1100 μm containing 100 μm of condensed fuel would have 39 fringes between its center and the inside of



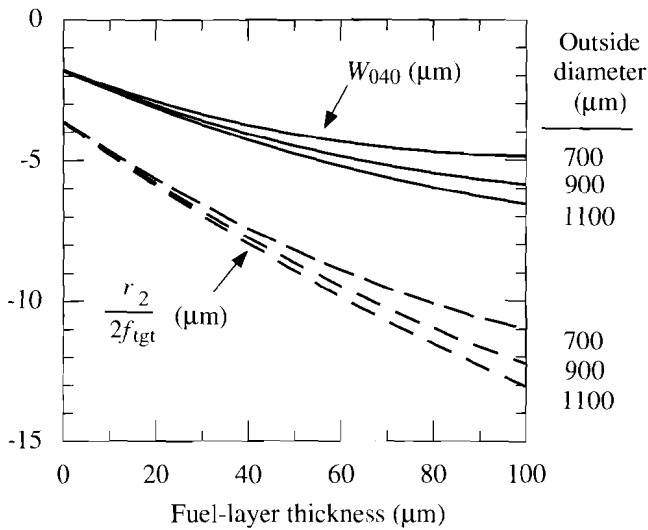
T1118

Figure 58.27

The effective focal length f_{tgt} of cryogenic targets as a function of condensed fuel-layer thickness. A 10- μm -thick polystyrene capsule was assumed for the various outside diameters shown. Paraxial rays were traced through hypothetical targets to find their focal lengths, which are measured from their equatorial plane.

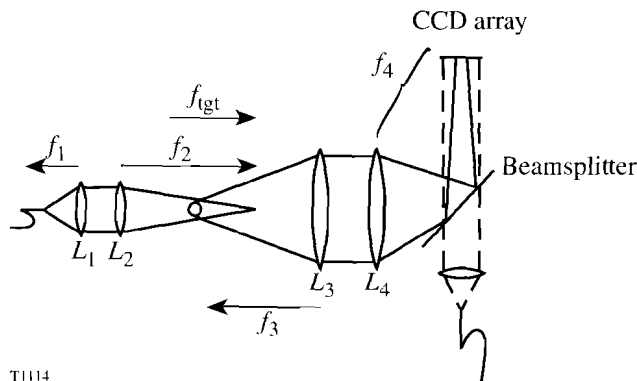
the fuel layer when planar wavefronts with a 0.5- μm wavelength are utilized to create its interferogram. Eliminating the spherical component of the emerging wavefront by illuminating the same target with a beam of light converging to its focal point 6.8 μm behind it produces only 13 fringes, which are mainly concentrated toward the perimeter of the image. Hence, a greater sensitivity to nonconcentricities and higher-order nonuniformities in the fuel layer can be achieved.

The optical system used to create an interferogram of a cryogenic target with convergent-beam illumination is shown in Fig. 58.29. (The properties of the light sources and components of the initial beamsplitting system shown in Fig. 58.30 will be discussed in detail later since their use will become more apparent following a description of the imaging system.) The light is delivered to the interferometer using two single-mode optical fibers, one for the object arm and another for the reference arm. The optical fibers serve several purposes. They vibrationally and optically isolate the laser source from the structural and optical components of the interferometer. In addition, the optical fiber's flexibility makes relative placement of the light source and the interferometer unrestricted. Transmitting only the lowest-order mode, the optical fibers also serve to spatially filter the light emitted by the laser source.



T1119

Figure 58.28
The values for $r^2/2f_{tgt}$ and W_{040} for cryogenic targets as a function of condensed fuel-layer thickness. Again a 10- μm -thick polystyrene capsule was assumed for the outside diameters shown. Third-order aberration theory was used to determine W_{040} . The values shown are for the emerging wavefront projected back into the equatorial plane of the target and denote the maximum values these quantities take, i.e., for $y = 1$.



T1114

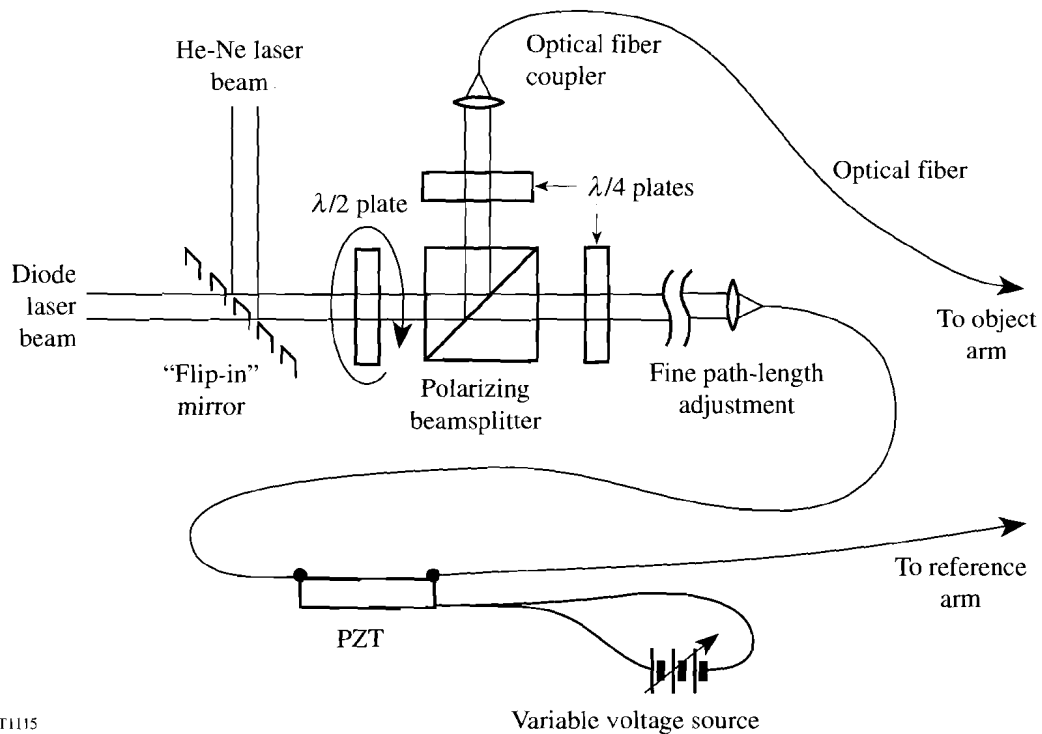
Figure 58.29
A schematic of the optical system used to create an interferogram of a cryogenic target with convergent-beam illumination. The optics that control the point of focus of the convergent beam and those that image the target are shown. The dotted line denotes the collimated reference beam.

The light emerging from the optical fiber in the object arm is first collimated with lens L_1 and is focused to a point with L_2 . All lenses in the interferometer are achromatic doublets corrected for infinite conjugates. All imaging takes place close to the optical axis of the interferometer, so the use of these lenses minimizes spherical aberration. Since the light between L_1 and L_2 is collimated, only the position of L_2 is adjusted to locate the focus of the convergent beam at the rear focal point of the cryogenic target.

The target is imaged onto a CCD array by the optical relay system composed of lenses L_3 and L_4 . The ratio of the focal lengths of these lenses, f_4/f_3 , determines the magnification of the imaging system. In some instances, the working distance between the target and L_3 (i.e., f_3) is required to be large, such as the case of imaging in the OMEGA Upgrade target chamber. For large magnifications, the required value of f_4 may then exceed the physical dimensions of the space allotted to this target diagnostic. In this case, f_4 can be made equal to f_3 , and a microscope objective lens can be used to further image the intermediate unity-magnification image of the target onto the CCD array.

The light emerging from the optical fiber in the reference arm of the interferometer is collimated, and the reference beam is combined with the object beam using a 50/50 beamsplitter. The partially reflective coating on the parallel-plate beamsplitter faces L_4 so that no aberration is introduced into the object beam by passage through a thick plate. Since the reference beam is collimated, its passage through the plate does not affect the planar reference wavefronts except to displace them laterally with respect to the optical axis of the collimating lens. The direction of propagation between the object and reference beams (i.e., the tilt) is controlled by rotating the reference beam's collimating lens about an axis perpendicular to its optical axis. Both the object and reference beams have a Gaussian, and therefore nonuniform, intensity profile upon emerging from the single-mode optical fiber. The centroid of the intensity distribution of the interferogram produced on the CCD array can also be positioned by translating the collimating lens in a direction perpendicular to its optical axis.

As the position of the focal point of L_2 is translated longitudinally with respect to the target's position, the irradiance of the object beam at the target (and its image) varies dramatically. The individual irradiances of the object and reference beams at the CCD array must be equal to produce interference fringes with the maximum possible contrast. Hence, to obtain high-contrast interferograms for a wide range of cryogenic target dimensions, the ratio of the power launched into the two fibers must be continuously variable. Referring to Fig. 58.30, this is accomplished using a polarizing beamsplitter in conjunction with linearly polarized laser light and a half-wave plate that can be rotated about its cylindrical axis. As the half-wave plate is rotated, the power ratio of the object beam to the reference beam varies continuously between 0 and 1.



T1115

Figure 58.30

A schematic of the optical system that divides the source of radiation into the object and reference beams. Variable wavefront division is possible using the half-wave plate and the polarizing beamsplitter. Polarization-preserving fiber is unnecessary if quarter-wave plates are used to circularly polarize the light launched into the single-mode optical fibers, thereby reducing the detrimental effects that the variable bending conditions of the fiber have on the interferogram.

When linearly polarized light propagates through an optical fiber that is not polarization preserving, the polarization direction of the light emerging from the fiber depends on the bending conditions of the fiber between the source and its termination. The contrast of an interference pattern also depends on the relative angle between the polarization directions of the two beams that produce it. To stabilize the interferogram's contrast, quarter-wave plates are used to launch circularly polarized light (with the same handedness) into each fiber. Although some ellipticity is introduced into the light's polarization during propagation through the fiber, the contrast remains relatively constant as the fibers' bending conditions change.

An interferogram created with long-coherence-length light generally contains a significant amount of low-contrast noise due to interference between reflections from the various optical surfaces. To reduce this noise, a source of short-coherence-length light can be utilized. However, this makes the alignment and optical-path balance between the object and reference beams more critical. GaAlAs gain-guided laser diodes operate with numerous longitudinal modes resonating simultaneously, producing radiation with a bandwidth of

several nanometers. This translates to a coherence length of only a few millimeters. To aid in alignment, the optical system is first aligned using a long-coherence-length source such as a He-Ne laser. When the maximum contrast of the interference fringes has been obtained by trimming the length of the optical fibers and adjusting the spacing between the polarizing beamsplitter and the optical-fiber coupler in the reference arm, the "flip-in" mirror in Fig. 58.30 can be removed and the laser diode becomes the light source. Fine path-length adjustment is accomplished by careful positioning of the optical-fiber coupler in the reference arm, which is mounted on a precision slide. A broadband polarizing beamsplitter and liquid-crystal wave plates that have an equal retardance for two wavelengths⁷ are used so the contrast of the interferogram is not altered when the light sources are interchanged.

Phase sensitivities of the order of a few hundredths of a fringe can be achieved using phase-shifting techniques.⁸⁻¹⁰ This involves sequentially acquiring multiple interferograms, each with a known phase offset between them caused by introducing a slight path-length change in one of the interferometer's arms. The phase of each point in the interferogram, modulo 2π , is then obtained by performing simple

mathematical operations on the set of interferograms. One advantage of phase-shifting methods is that the phase resolution depends primarily on the dynamic range of the CCD array (and the contrast of the interferogram) and, to a lesser degree, on the dimensions of individual pixels, as is the case with fringe-finding techniques.

An elegant method of introducing a controlled phase step into one of the interferometer's arms is to slightly elongate the optical fiber in that arm. This method introduces a path-length change alone and does not affect the tilt between the object and reference wavefronts, which can often be disturbed when an optical element such as a mirror or lens is displaced to introduce the same phase shift. A piezoelectric element to stretch the fiber and its associated electronics is commercially available in a single, compact unit.¹¹ The device is driven with a 0- to 10-V signal, which is compatible with typical digital-to-analog converters. The total phase shift introduced with respect to the maximum applied voltage can be selected by varying the total length of the fiber cemented to the piezoelectric element.

Typical interferograms produced with both plane-wave and convergent-beam illumination are shown in Fig. 58.31. To date, a laser diode has not been purchased, although suitable candidates have been identified. Therefore, both images in Fig. 58.31 were produced with a He-Ne laser. At this time, both large-diameter capsules and the methods to produce uniform, thick condensed fuel layers in them remain to be fully developed. Hence, tests were performed on room-temperature capsules with effective focal lengths comparable to those calculated for OMEGA Upgrade-sized capsules containing thick cryogenic fuel layers. Figure 58.31(a) was obtained by removing L_2 and adjusting the half-wave plate to produce maximum fringe contrast. In Fig. 58.31(b), L_2 was replaced and its position was adjusted until the center of the target's image was nearly uniform in intensity. Note that the f -number of L_2 must be chosen to sufficiently overfill the target's image so that the curvature of the object wavefront passing around the capsule can be accurately determined, as described below.

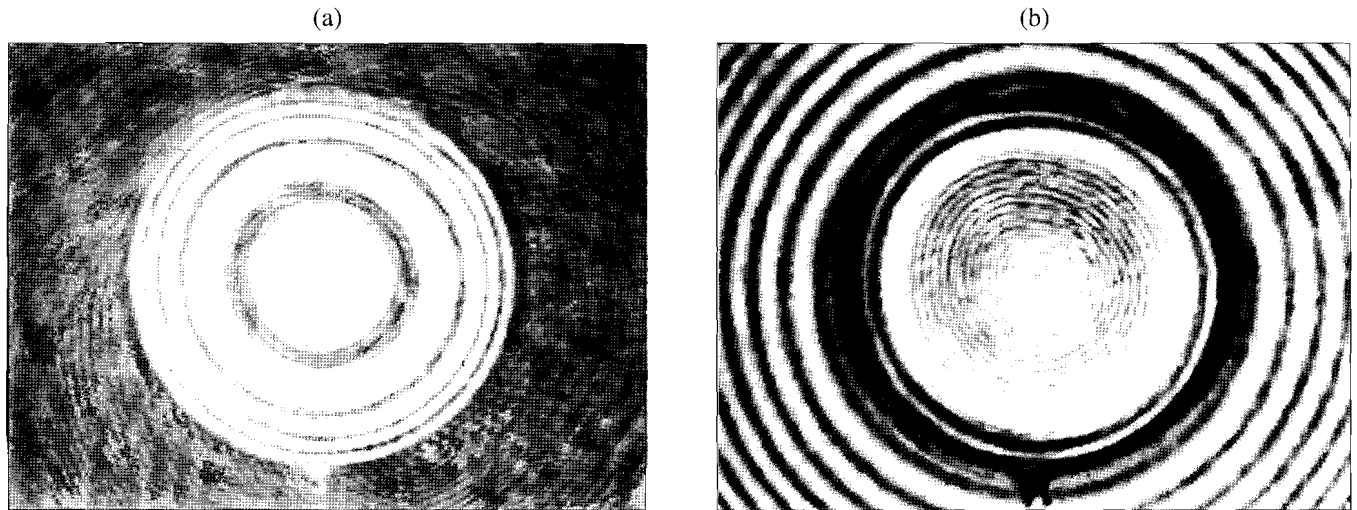
The interferogram shown in Fig. 58.31(b) is analyzed in the following manner to obtain information about the thickness and uniformity of the condensed fuel layer. First the center of the target's image is located while blocking the reference beam. The reference beam is restored, and phase-shifting techniques are utilized to map the phase of the wavefront as a function of position within the image, modulo 2π . The phase of the wavefront is "unwrapped" so that continuous surfaces

representing the wavefront inside and outside the target's image are obtained. The discontinuity between the wavefront transmitted through the capsule and that passing around it occurs near the circumference of the capsule, where there is a substantial step in the object wavefront's phase and there may be a dark area due to light being refracted outside the aperture of L_3 .

The wavefront within the interior of the capsule is then fitted to a set of polynomials that are orthonormal over a unit circle, such as Zernike polynomials.^{12,13} The center and radius of curvature of the wavefront surrounding the target's image is then determined. Although the background rings should be made concentric with the center of the target's image, the lateral displacement between the centroid of the target's circumference and the center of curvature of the wavefront surrounding the target's image determines the magnitude and direction of the residual tilt between the object and reference wavefronts. The difference in curvature of the wavefronts transmitted through and passing around the target is used to determine the thickness of the fuel layer, accounting for the contribution due to the empty capsule. The coefficients of the higher-order polynomials reveal the thickness and lateral dimensions of the nonuniformities present in the condensed fuel layer.

Although the analysis of the interferogram produced is significantly more complicated, the interferometer described above has several advantages over optical systems that illuminate the target with planar wavefronts. By illuminating the target with a beam converging to its rear focal point, the wavefront emerging from the target is flattened, with only the curvature due to the spherical aberration term remaining. More light is collected from regions near the perimeter of the target, and the interferogram consists of a set of rings that are concentrated near the perimeter of the target's image. This enhances the phase sensitivity, and therefore the sensitivity to thickness variations, that can be achieved with a specific CCD array.

In addition, this interferometer incorporates several unique features. The location of the convergent beam's focal point can be continuously adjusted to compensate for a wide range of capsule/fuel-layer dimensions. Stretching the optical fiber in the reference arm provides phase-shifting capabilities without translating optical components. The use of relatively short-coherence-length light suppresses interference from spurious reflections within the optical system, thereby reducing noise in the interferogram.



T1116

Figure 58.31

Actual interferograms of a 3.3- μm -thick glass capsule with a diameter of 270 μm . This capsule has the same focal length (-8.0 mm) as the target used to generate the interferograms in Fig. 58.24; however, W_{040} for the capsule in these images is only -0.55 μm instead of -6.5 μm for the comparable cryogenic target. The capsule was illuminated by a He-Ne beam and imaged by $f/3.5$ optics. In (a), L_2 was removed and the half-wave plate adjusted to produce maximum fringe contrast. L_2 was replaced in (b) and its position was adjusted until the center of the capsule's image was nearly uniform in intensity. Note the low-contrast noise in each due to interference between the reflections from the various optical surfaces and the relatively long coherence length of the light used.

ACKNOWLEDGMENT

This work was supported by the U.S. Department of Energy Office of Inertial Confinement Fusion under Cooperative Agreement No. DE-FC03-92SF19460, the University of Rochester, and the New York State Energy Research and Development Authority. The support of DOE does not constitute an endorsement by DOE of the views expressed in this article.

REFERENCES

1. J. A. Tarvin *et al*, in *Interferometry* (SPIE, San Diego, CA, 1979), Vol. 192, pp. 239–243.
2. T. P. Bernat, D. H. Darling, and J. J. Sanchez, *J. Vac. Sci. Technol.* **20**, 1362 (1982).
3. K. Kim, L. Mok, and M. J. Erlenborn, *J. Vac. Sci. Technol. A* **3**, 1196 (1985).
4. K. Kim and D. L. Krahn, *J. Appl. Phys.* **61**, 2729 (1987).
5. T. R. Pattinson and W. J. Felmlee, *J. Vac. Sci. Technol. A* **6**, 1882 (1988).
6. H. J. Kong, M. D. Wittman, and H. Kim, *Appl. Phys. Lett.* **55**, 2274 (1989).
7. Meadowlark Optics, 7460 Weld County Road 1, Longmont, CO 80504-9470.
8. K. Creath, in *Surface Characterization and Testing*, edited by K. Creath (SPIE, Bellingham, WA, 1986), Vol. 680, pp. 19–28.
9. K. Kinnstaetter, A. W. Lohmann, J. Schwider, and N. Streibl, *Appl. Opt.* **27**, 5082 (1988).
10. K. Creath, in *Progress in Optics XXVI*, edited by E. Wolf (Elsevier Science Publishers, 1988), pp. 349–393.
11. Canadian Instrumentation and Research Limited, 5035 North Service Road, Unit B7/8, Burlington, Ontario, Canada L7L 5V2.
12. M. Born and E. Wolf, *Principles of Optics*, 6th ed. (Pergamon, Oxford, 1980), pp. 464–468.
13. D. Malacara, ed., *Optical Shop Testing* (John Wiley & Sons, New York, 1978), pp. 489–505.